PHYSICAL REVIEW B **83**, 104205 (2011)

Neutron scattering experiments on liquid droplets using electrostatic levitation

T. Kordel,[1] D. Holland-Moritz,[1,*] F. Yang,[1] J. Peters,[2] T. Unruh,[2] T. Hansen,[3] and A. Meyer[1]

[1]*Institut für Materialphysik im Weltraum, Deutsches Zentrum für Luft- und Raumfahrt (DLR), 51170 Köln, Germany*

[2]*Forschungsneutronenquelle Heinz Maier-Leibnitz (FRM II), Technische Universität München, 85747 Garching, Germany*

[3]*Institut Laue-Langevin (ILL), 38042 Grenoble, France*

(Received 23 December 2010; revised manuscript received 3 February 2011; published 28 March 2011)

We present a compact electrostatic levitator as a sample environment for high quality neutron scattering experiments on melts. By this containerless approach we are able to investigate chemically highly reactive melts in a broad temperature range from high temperatures down to very low temperatures in the metastable liquid. The sample volume typical for former electrostatic levitation facilities was increased by one order of magnitude to a sample diameter of 6 mm. A minimized amount of scattering material in the vicinity of the neutron beam results in a low background of the device and thus in a significantly improved signal-to-noise ratio. Even in these large samples the temperature gradient induced by laser heating is less than 20 K. As a first result the Ni self-diffusion coefficient in $Zr_{64}Ni_{36}$ was measured by quasielastic neutron scattering at the time-of-flight spectrometer TOFTOF at the FRM II as a function of temperature. At an undercooling of 167 K below the melting point deviations from an Arrhenius-type temperature dependence as observed in bulk metallic glass forming alloys become evident. Neutron diffraction experiments were performed at the high flux diffractometer D20 at the ILL. With a neutron wavelength of 0.94 Å a high quality total structure factor of $Zr_{64}Ni_{36}$ was measured in a broad temperature range at wave numbers between 0.6 and 12 $Å^{-1}$.

DOI: 10.1103/PhysRevB.83.104205 PACS number(s): 61.25.Mv, 66.30.Fq, 61.05.fg

I. INTRODUCTION

Neutron scattering techniques allow us to study both the short-range structure and the atomic dynamics in liquids. Neutron diffraction provides information on the atomic structure of the liquid, which influences its macroscopic properties such as density, viscosity, surface tension, and electrical resistivity. The scattering strength of alloy components can be varied by isotopic substitution, which allows us even to determine a full set of partial structure factors that provide information both on the chemical and the topological melt structure. Partial structure factors can be used as input in numerical mode-coupling solutions to predict dynamic processes in the melts thus revealing details of the structure-dynamics relation in these systems.[1] Dynamic processes in the melt can be investigated by analyzing the scattering law $S(q,\omega)$ of quasielastic neutron scattering. The self-diffusion coefficients can be determined on an absolute scale with a low statistic and systematic error for elements with a sufficiently high incoherent scattering strength.[2] A precise knowledge of diffusion coefficients is, for example, a crucial input in the modeling of solidification processes.

As many melts are chemically highly reactive or have high melting temperatures, experiments in a container are often hampered by reactions of the sample with the crucible materials which change the composition of the melt and its properties. For weakly scattering samples the scattering signal can be dominated by the scattering of the container. In such cases containerless levitation techniques have to be applied for sample processing enabling neutron scattering experiments in a very broad temperature range up to very high temperatures. Due to the lack of container walls and impurities in the environment acting as heterogeneous nucleation sites,[3] the liquid can significantly be undercooled below the liquidus temperature in the levitation device. Hence temperature-dependent measurements can be extended into the metastable liquid state. As the amount of scattering material in the vicinity of the sample is reduced, containerless levitation techniques can also be employed to perform high quality neutron scattering experiments with reduced artefacts from spurious scattering and an excellent signal-to-noise ratio. An overview of the different levitation techniques is given in Refs. 3 and 4.

Since about ten years the electromagnetic levitation (EML) technique[5,6] as well as the aerodynamic levitation (ADL) technique[7,8] have been applied for elastic neutron scattering experiments on different kinds of melts. Very recently also quasielastic neutron scattering experiments were performed[9] using the EML technique with an improved coil design. An enlarged spacing between the coil windings increased the vertical detection angle of the scattered neutrons and reduced the background scattering from the coil resulting in an improved signal-to-noise ratio. Both levitation techniques have also been applied for diffraction studies using synchrotron radiation[10–14] and x-ray absorption spectroscopy investigations.[15,16] In the EML a sample is processed within an inhomogeneous radio frequency electromagnetic field. As levitation force and heating power are intimately coupled, the accessible temperature range is limited especially to low temperatures and a cooling gas is required. Moreover, only electrically conducting materials can be levitated. In the ADL the samples are levitated by a gas jet from below the sample. The typical sample size of 2–4 mm in diameter is small. Thermal gradients are induced in the sample by laser heating and the directional gas flow and the visibility of the sample is limited, as the sample is partly covered within the gas nozzle. As both techniques rely on a gas atmosphere they bear the risk of sample contamination by gas impurities.

These limitations of EML and ADL can be overcome by the electrostatic levitation (ESL) technique that was first successfully employed for the processing of melts by Rhim *et al.*[17] in 1993. Here gravity is balanced by the

electrostatic force acting on a charged sample in an electric field. Different from EML, the ESL technique is not restricted to conductive materials. The high purity conditions realized by processing under high vacuum are favorable for obtaining highest levels of undercooling.[18] The electrostatically levitated specimens are heated with a laser such that positioning and heating are decoupled and a temperature range from ambient temperature up to more than 2500 K is accessible. While the ESL technique has been used since nearly 10 years for performing containerless diffraction experiments using synchrotron radiation,[19,20] the early generations of electrostatic levitators were capable of levitating only comparatively small samples up to about 10 mm^3, such that the method was less attractive for neutron scattering studies. Moreover, when considering also the use of the levitator at neutron time-of-flight spectrometers, the geometrical constraints given by these instruments require a very compact facility design that is technically challenging. The principal feasibility of neutron diffraction experiments on electrostatically levitated samples has been demonstrated in 2003 by Aoki *et al.*[21] However, in that work only diffractograms recorded for solid samples are shown.

We have developed an ESL furnace dedicated for performing elastic and inelastic neutron scattering experiments on liquids that is able to levitate samples of about 100 mm^3. This means an increase of the scattering volume by about one order of magnitude as compared to earlier devices. We demonstrate for the example of liquid $Zr_{64}Ni_{36}$ that by use of this facility at the time-of-flight spectrometer TOFTOF of the Forschung-Neutronenquelle Heinz Maier-Leibnitz (FRM II) in Garching and at the high-intensity two-axis diffractometer D20 of the Institut Laue-Langevin (ILL) it is possible to record inelastic as well as elastic neutron scattering data of highest quality on electrostatically levitated metallic melts, even in the metastable regime of a deeply undercooled liquid.

II. APPARATUS

A schematic sketch of the electrostatic levitation furnace for neutron scattering is shown in Fig. 1. Figure 2 shows the levitation device situated in the neutron scattering environment. An electrically charged sample (*S*) is levitated in the electric field of two vertically arranged electrodes (TE,GE) supplied with a high voltage such that the electrostatic force compensates for the gravitational force. According to Earnshaw's theorem, in a static electric field without space charges no potential minimum exists.[22] Therefore the sample position needs to be actively controlled in all three directions in space. In addition to the vertical control by the top and ground electrode, the horizontal sample position is controlled by two pairs of side electrodes (SEs).

The sample position is monitored by the shadow the sample casts in two crossed expanded laser beams on position-sensitive photodetectors (PSDs). Gaussian beams of two diode lasers (30 mW at 660 nm, Schäfter+Kirchhoff) are guided by a polarization maintaining single mode fiber to the outcoupling optics. The collimated beams with a diameter of 2.2 mm are expanded by beam expanders (BEs, Qioptiq) with a magnification of 25 and 50, respectively to get homogeneous illumination between the electrodes. With a variable iris

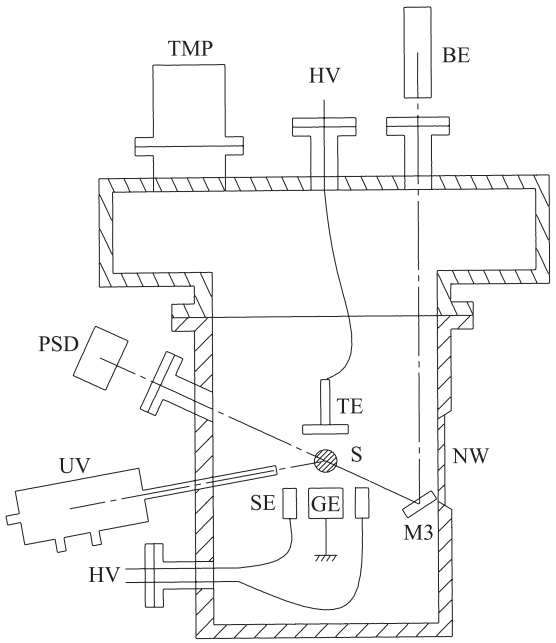

FIG. 1. Schematic drawing of the levitation chamber, vertical cut. Top electrode: TE; ground electrode: GE; side electrode: SE; sample: S; beam expander for laser: BE; mirror: M3; position sensitive detector: PSD; high voltage feedthrough: HV; turbo molecular pump: TMP; UV lamp: UV; neutron window in vacuum chamber: NW.

aperture the beam diameters can be adjusted to the electrode spacing. To allow for a compact facility with little material in the vicinity of the sample and a large free-scattering angle, two perpendicular position laser beams are introduced from the top in the chamber and reflected by mirrors on the sample. Two mirrors (M1, M2) are located in the scattering plane reflecting the beam onto the sample and on the detector at the top of the chamber (Fig. 2). Another mirror (M3) is located below the scattering plane and reflects the laser beam on the sample which then directly passes to the detector (Fig. 1). To minimize the shading of this laser beam by the horizontal electrodes, the electrodes are turned by 45° with respect to the laser beams such that the laser passes between the horizontal electrodes. In the position control algorithm the measured horizontal coordinates are then transformed to the coordinate system of the electrodes by a rotation matrix. With this concept a range of 130° of unshaded scattering angle is realized.

The sample shadow in the laser beam is measured by two Si based position-sensitive photodetectors with an active area of 20×20 mm^2 (SiTek electro optics). Each measures the movement in two perpendicular directions. To minimize the influence of scattered light and light from the bright sample at high temperatures, the detector is protected by a polarization filter and a bandpass interference filter matched to the position laser wavelength. The photocurrents for both perpendicular directions are amplified and converted into a proportional voltage by a dual-axis position sensing amplifier (amplification $10^{(-4)}$ A/V, on-trak photonics).

The position signal is the input for a closed-loop sample position control algorithm[23] adjusting the high voltage supplied to the electrodes every 2 ms. The algorithm is defined by two sets of three control parameters for the horizontal and vertical

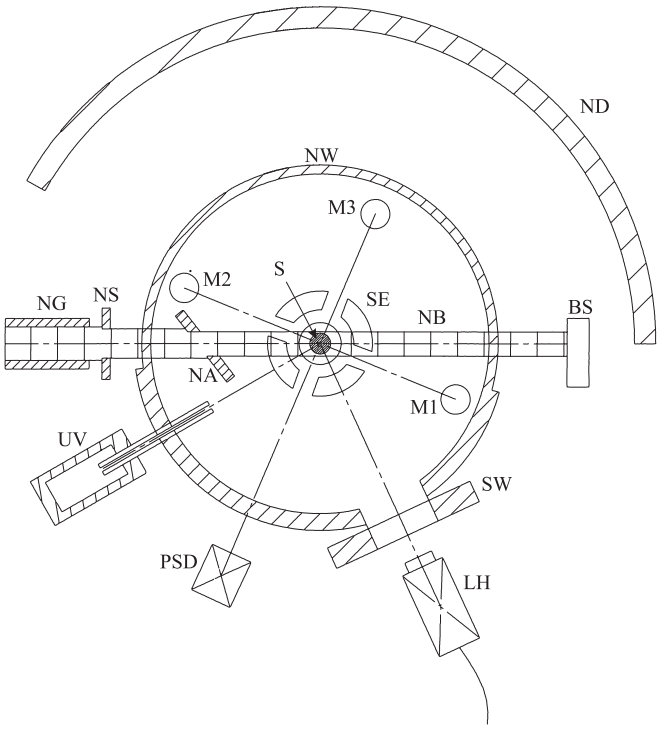

FIG. 2. Schematic drawing of the levitation chamber in the neutron scattering environment, horizontal cut. Position sensitive detector: PSD; mirror: M1-3; side electrodes: SE; high voltage feedthrough: HV; UV lamp: UV; laser head containing the outcoupling optics of the heating laser, the pyrometer, and the charge-coupled device (CCD) camera: LH; window for sample exchange: SW; neutron window in vacuum chamber: NW; neutron beam guide: NG; neutron slit system: NS; neutron B_4C- aperture: NA; neutron beam: NB; neutron beam stop: BS; neutron detector: ND.

directions. These parameters depend on the mass and the radius of the sample and have to be carefully tuned for stable levitation behavior. An executable of the control algorism is then built in MATLAB/SIMULINK on a host computer. It is then transferred on a target computer where the algorism is executed by xPC Target in real time. For the levitation against gravity a high-voltage amplifier of 40 kV maximum voltage (Trek, PM07071N) is used. For horizontal position control the four channels of the bipolar high-voltage amplifiers (highvolt, HVA 3B4, 3kV) are operated in two pairs of equal voltage but opposite polarity.

To realize a clean environment and to avoid electrical breakthrough of the high voltages the electrodes are placed in high vacuum. For heating of the samples a 75 W infrared fiber coupled diode laser, type Mergenthaler ML75 with a wavelength of 808 nm, is used, which is sufficient to melt metals with high melting temperatures above 2000 K, such as Zr. In the outcoupling optics a fiber coupled two-color pyrometer for contactless measurement of the sample temperature and a charge-coupled device (CCD) camera (LH) for observation of the sample are mirrored in the same beam path for compact design and convenience in laser adjustment. The pyrometer works at the two wavelength ranges from 1650 to 1750 nm and 1850 to 2000 nm. To ensure laser safety the levitation chamber is hermetically closed. All openings are secured by safety interlocks.

The wavelength of 808 nm is well absorbed by metals. Due to the low absorption of liquid ceramics and oxides at this wavelength for processing of those materials the 10.6 μm laser wavelength of a CO_2 laser has to be applied. To include a CO_2 laser into the current setup the sample window could be equipped with a flange adapter for two windows, a standard vacuum window for the pyrometer and the camera, and a ZnSe window for the CO_2 laser. With a spherical Au mirror in front of the window the laser beam could be focused onto the sample.

The evaporation of sample material during heating is associated with a reduction of the total charge of the sample. Because the high voltage is limited, charge loss has to be compensated to maintain stable levitation. Therefore the positively charged sample is illuminated by ultraviolet light and recharged via the photoelectric effect. As source of the UV light (UV) a He discharge lamp (Specs, UVS10/35) is utilized. The lamp unites a compact design with high photon energy (20 eV) and a high photon flux. A discharge arc is ignited by high voltage (1.5 kV) in a He gas flow of approx. 1 mbar pressure. As no transparent window material exists for that photon energy the ignition chamber of the lamp is directly connected to the main chamber of the levitator. A thin capillary of 1 mm diameter points toward the sample and is pumped differentially at two stages allowing for a gas pressure up to 10^{-7} mbar in the main chamber. At elevated temperatures (around 1200 K) thermionic emission becomes an efficient charging mechanism such that charging by irradiation with UV light is not required anymore. In order to avoid pollution of the UV lamp due to higher evaporation rates of the sample at higher temperatures the capillary is protected with a mechanical shutter.

One of the major challenges of the facility design was the adaption of the ESL technique to the physical and geometrical requirements of neutron scattering experiments. Especially the desired use at time-of-flight spectrometers required a very compact facility design. Moreover, the sample size was an issue since for the ESL facilities used so far the typical sample sizes are 2–3 mm in diameter. Due to the limited neutron flux in neutron scattering experiments the aim was to enlarge the sample size and therefore the scattering volume to ensure good statistics in a reasonable measuring time. To levitate samples with higher masses higher electric fields are required and larger electrode spacings had to be realized. When increasing the maximum vertical positioning voltage from 20 kV (employed in former devices) to 40 kV, sparkling even in high vacuum and field emission of electrons had to be overcome. We are now able to levitate a sample of up to 6.5 mm in diameter (Fig. 3). This means that we increased the typical mass of the samples and therefore the scattering signal by one order of magnitude from usually 50–100 mg to 0.5–1 g. For improved visibility of the sample the electrode spacing was increased from 8 to 12 mm. The signal-to-background ratio was further increased by the use of electrodes made of low scattering and neutron absorbing Al 8 wt % B alloy.

The vacuum chamber is equipped (mainly) with conflate flanges. With a turbo molecular pump, type Leybold Turbovac 361 (TMP) backed with a Scroll pump (Scrollvac SC15D) a pressure in the 10^{-7} mbar regime can be reached within 1 h. The upper part of the chamber consists of stainless steel. A valve for flooding the chamber with dry gas before

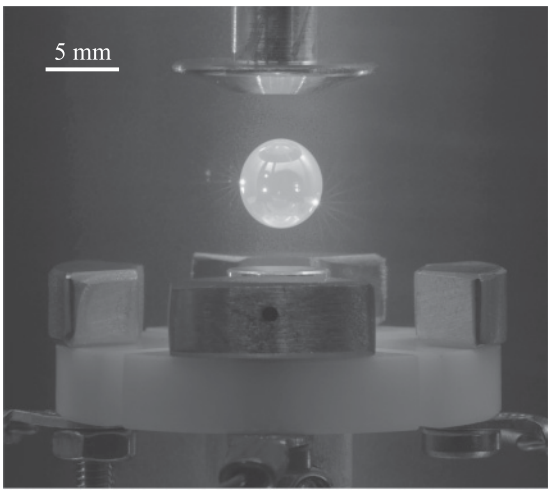

FIG. 3. Liquid sample ($Ti_{39.5}Zr_{39.5}Ni_{21}$, 0.6 g) processed in the ESL at 1123 K.

sample exchange, a pressure gauge, and a 40 kV high-voltage feedthrough (HV) for the supply of the vertical positioning voltage is mounted on the top of the chamber. Two windows allow the laser beams for position detection to enter the chamber. One window is backed with a photosensitive detector. The lower part of the vacuum vessel is made of the low scattering and low absorbing aluminium alloy AlMgSi, equipped with Atlas bimetal conflate flanges. It has a DN150CF window for sample exchange, heating, pyrometry, and monitoring. In future upgrades also a second laser outcoupling optics can be installed for heating and pyrometry from the back side of the sample via a mirror. Additionally there are three DN40CF flanges: one for mounting the four-port high-voltage feedthrough (HV) for the voltage supplied to the side electrodes, a port for the UV lamp (UV), and a window for another position-sensitive detector (PSD).

The neutron beam adjusted in size by the slit systems (NS) at the end of the beam tube enters the vacuum chamber through an Al window. The neutron window (NW) is machined into the aluminium container wall and has a thickness of 2 mm. It covers 220° horizontally and ±20° vertically. A densely sintered neutron absorbing B_4C aperture (NA) shapes the beam again in the chamber right in front of the sample. Apertures of different diameters are available but typically an aperture of 8 mm is used, which is larger than the sample to ensure scattering at the entire sample, but it is smaller than the electrode spacing to minimize the background level. The aperture has an angle of 45° with respect to the incident neutron beam to ensure that the range of high scattering angles is not obstructed by the aperture. In the diffraction experiment at D20 the direct neutron beam is blocked inside the chamber by a Cd beam stop (BS) to avoid secondary scattering from the exit neutron window (NW).

III. FACILITY PERFORMANCE

A. Position stability

The position stability of the sample influences the quality of scattering experiments. For quasielastic neutron scattering a displacement of the sample from the scattering center will change the path length to the detector and thus broaden the energy resolution. In diffraction experiments a shift of the sample position will change the scattering angle and therefore change the wave number. Nevertheless, taking into consideration the large sample-detector distances typical for neutron scattering experiments, here even sample movements of about 1 mm are acceptable. Such a positioning stability can be easily realized by all state-of-the-art levitation technologies. Moreover, the measured intensity is dependent on the irradiated sample volume and the pathway of the radiation through the sample. Hence the intensity is affected by the sample position. The intensity measurement is robust against small sample movements, if non-moving position-sensitive detectors are used, that allow for a simultaneous measurement in the whole range of momentum transfers, if essentially the whole sample is illuminated with a wide beam and if weakly interacting radiation (e.g. neutrons) is used. The same is the case for energy-dispersive x-ray diffraction setups, because here all x-rays acquired at a given time by the energy dispersive detector traveled the same pathway through the sample. By choice of such robust scattering approaches, even the comparatively fair position stability of electromagnetic levitation facilities is sufficient to allow for diffraction studies on liquids of highest quality. The situation, however, is different in angle dispersive x-ray diffraction experiments using monochromatic synchrotron radiation. Due to stronger interaction of x-rays with matter, the intensity measured under a given scattering angle is strongly dependent on absorption within the sample. In order to correct for the angle dependence of the absorption, a well defined scattering geometry and hence an exact sample position control is of fundamental importance.

The absolute position stability of a liquid sample in the ESL was measured using video analyzing software. From a video 25 black-and-white pictures per second are extracted. With an algorithm the edge of the bright sample is detected by the gray value difference of adjacent pixels. Then the position of the edge pixel is fitted with a polynomial. A shift of the center of the detected area corresponds to a movement of the sample. The amplification of the optical imaging is normalized by the electrode spacing. The sample movement is plotted in Fig. 4 as a function of time. In order to test the response to external disturbances we excited a displacement of the sample from the center position by a mechanical impact on the facility at time $t = 0$ s. The control algorithm reacts on the displacement by increasing the electric field in the horizontal direction pushing back the sample to the center position. The resulting oscillation in the sample position is then damped away within a few seconds. The required voltages are well within the dynamic range of the high-voltage amplifiers of the side electrodes of ±3 kV. Before the excitation, the variation of the center position of the sample shows that the positioning with the control algorithm is very smooth and accurate. Without external perturbation the relative position stability of the liquid sample is better than ±10 μm.

The electrostatic force suspending the sample between the top and ground electrodes elongates the spherical shape of the liquid droplet along the vertical axis (cf. Fig. 3). The elongation depends on the surface tension of the alloy, the mass and the size of the sample, and the position in the electric field. For

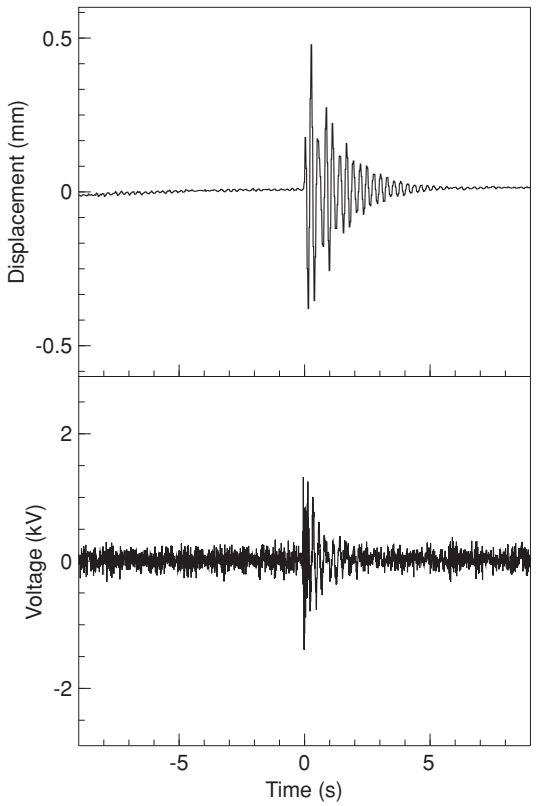

FIG. 4. Horizontal displacement of the sample (upper diagram) and levitation voltage supplied to the side electrodes (lower diagram). The variations around the center position for $t < 0$ s are less than 20 μm. The horizontal excitation at $t = 0$ s is damped within a few seconds providing an excellent position stability of samples in the ESL of about ± 10 μm.

$Zr_{64}Ni_{36}$ of 0.6 g the semimajor is about 10% larger than the semiminor.

B. Temperature measurement

While in the EML the samples are heated homogeneously on the entire sample surface in the ESL, the laser heating deposits all the power on a spot (here about 1 mm in diameter). Therefore thermal gradients are induced in the sample. To estimate the maximum temperature difference in the sample we measured the temperature with the pyrometer that is built in the laser unit and measures the temperature on the laser spot and simultaneously with an additional pyrometer on the back side of the sample. The thermal radiation of the sample obeys the Stefan-Boltzmann law $P(T) = \epsilon A \sigma\ T^4$, with P the radiated power, ϵ the emissivity of the sample surface, A the surface area, σ the radiation constant, T the temperature of the sample. As the radiated power strongly depends on temperature, the temperature gradient will increase at high temperatures. The temperature gradient also grows with increasing mass of a sample as the radiated power depends on the surface area. To give values for the temperature inhomogeneity a large sample (750 mg, 6 mm diameter) and a medium sample (500 mg, 5.2 mm diameter) of liquid $Zr_{64}Ni_{36}$ were processed. Due to limited heat conduction and low convection in this dense melt, large differences can build up. For calibration of the

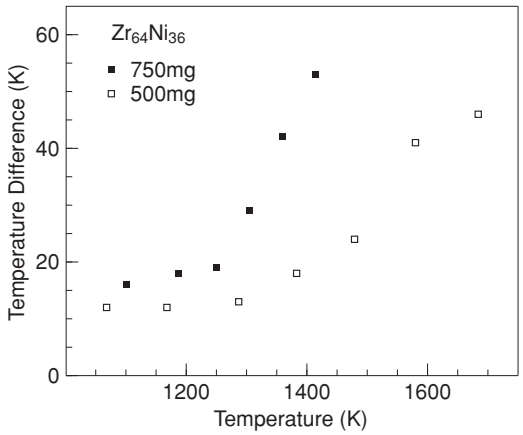

FIG. 5. Temperature difference of the heated front side and the back side of a large sample (750 mg, 6 mm diameter) and a medium sample (500 mg, 5.2 mm diameter) of $Zr_{64}Ni_{36}$ as a function of temperature.

two pyrometers we use the plateau of recalescence in the temperature-time profile when the liquid sample cools freely without laser heating. When the sample crystallizes from the metastable undercooled state, heat of crystallization is released increasing the temperature of the entire sample instantaneously to the liquidus temperature. The temperature remains constant until the entire sample is crystallized. When the liquid sample cools freely (without laser heating) for several tens of seconds from high temperatures into the undercooled regime, temperature gradients will be equilibrated. Indeed both pyrometers show temperature differences of less than 3 K during free cooling, confirming the temperature calibration.

The measurements (Fig. 5) show that the temperature inhomogeneities are small in the undercooled liquid and the inhomogeneities increase at higher temperatures, especially for the large sample. The temperature differences are less than 20 K for the medium sample up to a temperature of 1400 K and below the melting temperature for the large sample. This corresponds to a deviation of ± 10 K or less than $\pm 1\%$ from the average temperature of the sample. The temperature differences rise up to about 50 K at 1440 K for the large sample and about 40 K at 1600 K for the medium sample.

To reduce the temperature inhomogeneities at high temperatures further, a second laser will be used to heat the sample additionally from the back side of the sample. The vacuum chamber is designed such that a second heating laser can be implemented in the setup easily.

IV. NEUTRON SCATTERING EXPERIMENTS

A. Quasielastic neutron scattering

Quasielastic neutron scattering experiments were performed at the time-of-flight spectrometer TOFTOF at the FRM II (Refs. 24 and 25) for liquid $Zr_{64}Ni_{36}$ in a broad temperature range from high temperatures down to temperatures in the undercooled melt below the liquidus temperature ($T_{\mathrm{Liq}} = 1283$ K). The samples are prepared from 99.995% pure Zr and 99.999% pure Ni alloyed in an arc melting furnace

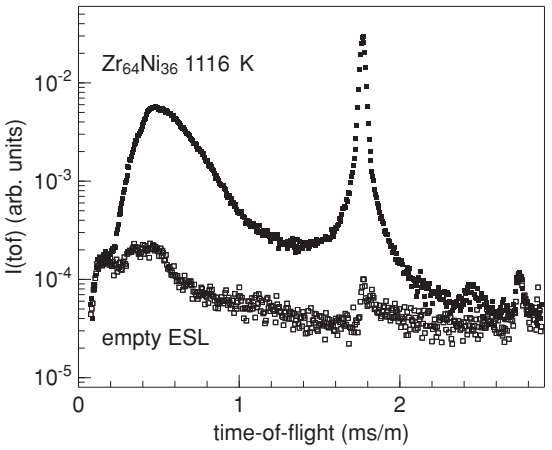

FIG. 6. Time-of-flight spectrum of a liquid $Zr_{64}Ni_{36}$ sample (mass 0.6 g) 167 K below melting temperature and the spectrum of the empty ESL recorded with a neutron wavelength of 7 Å. The spectra are normalized for detector efficiency and monitor counts and spectra from 17° to 130° scattering angle are integrated. Please note the logarithmic scale of the intensity axis in the diagram.

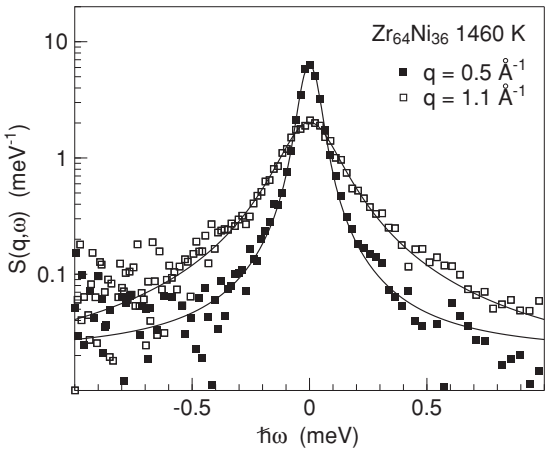

FIG. 7. Scattering law $S(q,\omega)$ of $Zr_{64}Ni_{36}$ at 1460 K for $q = 0.5$ Å^{-1} and $q = 1.1$ Å^{-1} fitted with Lorentzians. The width of the Lorentzian increases with increasing wave number q.

within an inert gas atmosphere of 99.999 9% Ar. In Fig. 6 the intensity $I(\text{tof})$ of the scattered neutrons of liquid $Zr_{64}Ni_{36}$ (mass 0.6 g) at 1116 K and of the empty instrument is plotted as a function of time-of-flight (tof) normalized to the flight path distance. The spectra are recorded using an incident neutron wavelength of 7.0 Å. They are normalized to detector efficiency and monitor counts only. The plotted spectra are integrated over a range of scattering angles from 17° to 130°. Due to the containerless processing method, the background signal is approximately two orders of magnitude below the sample signal.

From the scattering intensity $I(2\theta,\text{tof})$ the scattering law $S(q,\omega)$ (Fig. 7) is calculated.[28] The quasielastic peak is well described by a Lorentzian convoluted with the instrumental resolution. From the scattering signal of Vanadium at room temperature with a chopper speed of 8000 rpm and frame overlap ratio of 3 an instrumental resolution with a full width at half maximum of 55 μeV is determined. At small wave numbers ($q < 1.2$ Å^{-1}) the signal is dominated by incoherent scattering of the Ni atoms [$\sigma_{\text{inc}}(\text{Ni}) = 5.2$ b and $\sigma_{\text{inc}}(\text{Zr}) = 0.02$ b]. For incoherent scattering the full width at half maximum of the Lorentzian Γ is related to the self-diffusion coefficient D of the incoherent scattering atoms by the equation $D = \Gamma/(2\hbar\, q^2)$.[29,30] Thus from the slope of the $\Gamma(q^2)$ curves at small wave numbers the Ni self-diffusion is deduced.

In Fig. 8 the temperature dependence of the Ni self-diffusion coefficients in liquid $Zr_{64}Ni_{36}$, measured using the ESL technique as well as the EML technique,[26] is shown. The values determined with the ESL compare well with the values measured with the EML. Due to the clean environment in the high vacuum of the ESL we were able to extend the temperature range to lower temperatures. Neutron data for about 20 min were collected at 1116 K, which is 167 K below the melting point (see Fig. 6). In Fig. 8 also the average Ni and Ti self-diffusion coefficient[31] of the bulk metallic glass forming alloy Vit1 is plotted at low temperatures. The addition of other components (Ti, Cu, Be) to the Zr-Ni alloy decreases the liquidus temperature and improves the glass formation ability and undercoolability. Surprisingly it only has a minor influence on the Ni self-diffusion. A similar effect has been observed in the system Ni-P, in which the addition of Pd and Cu only has a minor impact on the self-diffusion of Ni in Pd-Ni-Cu-P.[32] In such metallic glasses mode coupling theory predicts a $[(T - T_c)/T_c]^{\gamma}$ temperature dependence[28] of the self-diffusion coefficient when approaching a critical temperature T_c. The solid line is a fit of the scaling law to the Vit1 data with $T_c = 850$ K and $\gamma = 2.5$.[27] In the diffusion data obtained with the ESL, small deviations from the Arrhenius-type temperature dependence $D(T) = D_0 \exp(-E_A/k_B T)$ with $E_A = (0.64 \pm 0.02)$ eV and $D_0 = (2.1 \pm 0.3) \times 10^{-7}$ m^2/s (dashed line) become evident at the highest undercoolings indicating approaching the critical temperature.

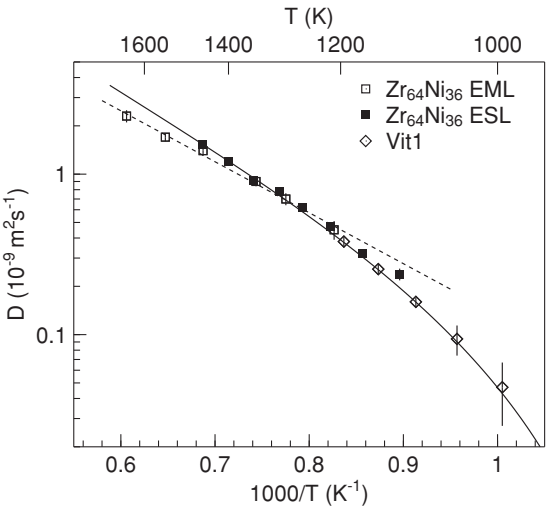

FIG. 8. Temperature dependence of the Ni self-diffusion coefficient in liquid $Zr_{64}Ni_{36}$ processed by the EML (Ref. 26) and the ESL technique and the average Ni and Ti self-diffusion coefficient (Ref. 27) in the bulk metallic glass forming Vit1 alloy. The solid line represents a fit of a T_c scaling law to the Vit1 data with $T_c = 850$ K and $\gamma = 2.5$ (Ref. 27).

B. Diffraction

Elastic neutron scattering experiments on liquid $Zr_{64}Ni_{36}$ were performed at the high flux diffractometer D20 (Ref. 33) at the Institut Laue-Langevin using a wavelength of 0.94 Å. In order to reduce the background intensity the oscillating radial collimator has been used. The scattering signal of a $Zr_{64}Ni_{36}$ sample of 0.6 g at $T = 1085$ K normalized to monitor counts and corrected for the detector efficiency only is plotted in Fig. 9 together with the background signal of the empty levitator. At scattering angles $2\theta < 10^\circ$ the background signal strongly increases due to the vicinity of the primary beam. The angular range of $2\theta < 4^\circ$ is covered by the beamstop of Cd, which leads to a significant drop of the intensity (however, not to zero due to the finite absorption of the Cd beam stop). At $2\theta > 134^\circ$ the intensity of the sample drops due to absorption of a positioning mirror within the vacuum chamber. Thus wave numbers from approximately 0.6 to 12 $Å^{-1}$ are accessible at a wavelength of 0.94 Å. In the usable range of momentum transfer the scattering intensity of the sample is about one order of magnitude stronger than the background. The static total structure factors of liquid $Zr_{64}Ni_{36}$ are determined from the measured diffractograms using the data treatment procedure described in detail in Ref. 6. The differential scattering cross section is obtained by subtracting the spectrum measured at the empty levitation furnace (without the sample) from the measured spectrum of the sample inside the furnace. A self-absorption correction according to the method of Paalman and Pings,[34] Placzek correction for inelastic scattering,[35] a normalization using a vanadium reference sample, and a standard multiple scattering correction are carried out. The spectrum is then normalized using a constant factor that is adjusted such that its asymptotic value at large q coincides with the total scattering cross section $\sigma_{tot} = \sigma_{inc} + 4\pi\langle b^2\rangle$ with σ_{inc} denoting the incoherent scattering cross section and b the coherent scattering length. $S(q)$ is then obtained by subtracting the incoherent scattering and a magnetic contribution.

The structure factors determined by means of this method for liquid $Zr_{64}Ni_{36}$ are shown for different temperatures in Fig. 10. The peak positions and the general shape of the

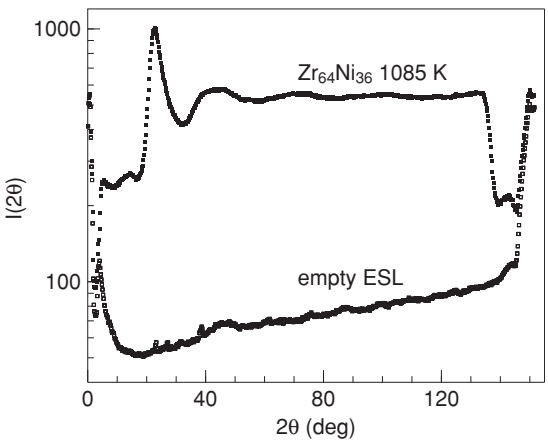

FIG. 9. Diffractogram of liquid $Zr_{64}Ni_{36}$ (0.6 g) measured at 1085 K using a neutron wavelength of 0.94 Å. The background of the empty ESL is one order of magnitude lower than the signal of the sample.

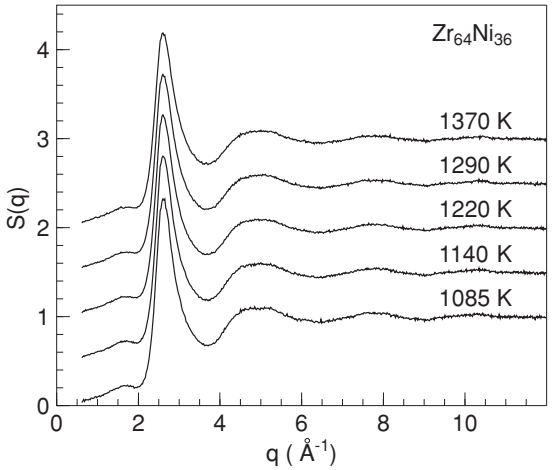

FIG. 10. Total static structure factor of liquid $Zr_{64}Ni_{36}$ for different temperatures in the stable liquid and down to about 200 K below the melting temperature ($T_{Liq} = 1283$ K). The structure factors are shifted by multiples of 0.5 for clarity.

structure factor do not significantly change with temperature indicating that the short-range order remains essentially unchanged. Small changes with temperature can be observed in the amplitudes of the oscillations. As observed also for other metallic melts,[5,36] the characteristic features of the structure factors become more pronounced, if the temperature is decreased. Recently we have investigated the short-range order of stable $Zr_{64}Ni_{36}$ melts at $T = 1375$ K at the same diffractometer (D20), however, using the electromagnetic levitation technique.[26] Isotopic substitution of Ni allowed us to determine even partial structure factors. While the partial structure factors have been determined at one temperature above the melting temperature, here we have demonstrated that there is no significant change of the short-range order in the investigated broad temperature regime ($1085\ \text{K} < T < 1370$ K). For a direct comparison of the results obtained using the two different levitation setups, in Fig. 11 the total static structure factor measured with natural Ni using the EML technique and that measured at essentially the same temperature ($T = 1370$ K) by application of the electrostatic

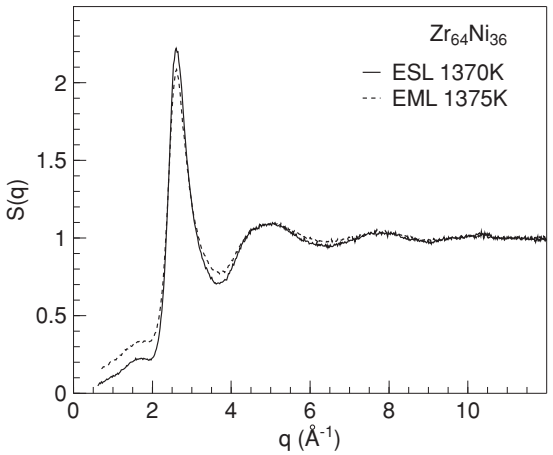

FIG. 11. Total static structure factor of $Zr_{64}Ni_{36}$ using the EML and the ESL techniques. Differences are discussed in the text.

levitator are plotted. While both curves have the same shape it is evident that the oscillations in the structure factor measured by ESL are slightly more pronounced. The first maxima of both structure factors differ by approximately 5% in height. This difference may result from contributions of secondary scattering where scattered neutrons subsequently also scatter at parts of the sample environment. Because such contributions to the measured intensity only occur if a sample is irradiated, they are not removed by the background subtraction using the signal measured with the empty levitator. For the ESL there are only the electrodes that are made from low scattering and absorbing Al 8 wt % B in the vicinity of the sample, such that secondary scattering should be negligible. For the EML, however, the sample is levitated within a water-cooled Cu coil. Especially due to the high incoherent scattering cross section of water, some incoherent background from secondary scattering cannot be ruled out for the EML measurement. This contribution should—in principle—be subtracted from the data before the above-mentioned normalization to σ_{tot} is performed. As the contribution cannot be quantified by EML measurements alone, the effect could not be considered during data treatment. For the case of a significant contribution to the measured intensity by secondary scattering, this results in a decrease of the amplitudes of the oscillations of the signal after normalization to σ_{tot}, which explains the observed differences in the structure factors measured using the ESL and the EML. If it is assumed that the incoherent contribution from secondary scattering amounts to only about 10% of the intensity measured at large q and if this contribution is subtracted from the EML data, a good agreement between both measurements can be achieved. Moreover, the extrapolation to $q \rightarrow 0$ point to a more realistic order of magnitude for the isothermal compressibility in the case of the ESL data.

In order to discuss the consequences of secondary scattering problem for the analysis of the short-range order of the melt, we calculate the total pair-correlation functions $g(r)$ from the total structure factors of Fig. 11. While this will allow us to analyze the influence of the error due to secondary scattering, we are aware that for a careful analysis of the chemical and topological short-range order of an alloy melt, partial structure factors and the corresponding partial pair-correlation functions must be determined as performed by our isotopic substitution experiments using the EML technique.[26] The total pair-correlation functions determined for $Zr_{64}Ni_{36}$ using the ESL and the EML techniques are plotted in Fig. 12. Again both curves differ only in the amplitude of the oscillations. Hence the interatomic distances inferred from both measurements are identical. Also the influence on the coordination numbers calculated from $g(r)$ is negligible due to the fact that the smaller amplitude in the maxima of the EML data is compensated by less deep minima. Because for alloy melts coordination numbers should be correctly calculated from partial pair-correlation functions and not from total ones, we refer to Ref. 26 for absolute values.

The observed reduction of the amplitude of the oscillations of the structure factor in the order of about 5% in EML data may be relevant when directly comparing these data, for instance, with MD simulation data. Nevertheless, the above discussion clearly shows that despite the limitations of the EML technique due to secondary scattering at the water-cooled levitation coil, the main results on the short-range order are essentially not affected by these problems.

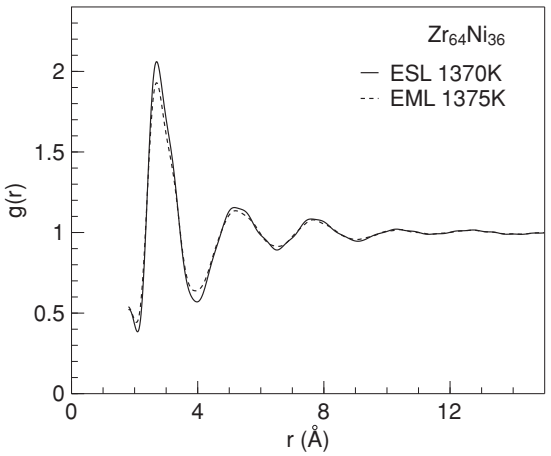

FIG. 12. Total pair-correlation function of $Zr_{64}Ni_{36}$ using the EML and the ESL techniques.

C. CONCLUSIONS

We have developed an electrostatic levitation furnace for containerless neutron scattering experiments on stable and undercooled melts. Using this sample environment we have performed quasielastic neutron scattering experiments at the time-of-flight spectrometer TOFTOF at the FRM II and at the high-intensity diffractometer D20 of the ILL. We have demonstrated that by means of this electrostatic levitation device dynamic and static structure factors of highest quality can be measured. Due to the containerless processing setup and the process under high vacuum conditions, high levels of undercooling are possible and the metastable state of the undercooled liquid can be maintained for extended periods of time sufficient to record neutron data with excellent statistics. Moreover, the recorded spectra are characterized by an excellent signal-to-background ratio due to the containerless approach. The electrostatic levitation technique is complementary to other containerless processing methods up to now used for neutron scattering experiments such as electromagnetic and aerodynamic levitation, enabling new possibilities for neutron scattering experiments on liquids.

While the sample environment was primarily designed to meet the requirements of neutron scattering experiments, it is also well suited for diffraction studies on the short-range order of liquids and on the phase selection during solidification of (undercooled) melts using high-energy synchrotron radiation. The ESL has a high position stability, the thin scattering window of Al shows a low absorption for high-energy x-rays and the compact dimensions of the furnace are well compatible with existing setups at synchrotron radiation beamlines. Such x-ray diffraction experiments on (undercooled) melts have successfully been performed utilizing ESL,[19,20] but also ADL[11,37] and EML.[12–14]

By quasielastic neutron scattering the Ni self-diffusion coefficient in liquid $Zr_{64}Ni_{36}$ has been measured with high accuracy in a broad temperature range. Different from the temperature dependence of the self-diffusion coefficients in

pure liquid Ni (Ref. 9) or Cu (Ref. 2) a deviation from an Arrhenius-type temperature dependence was detected at very low temperatures 167 K below the melting temperature as observed in multicomponent bulk glass forming alloys. In elastic neutron scattering experiments the total static structure factor has been measured in a broad temperature range, which does not change significantly. Differences can be seen comparing the structure factor of $Zr_{64}Ni_{36}$ using the EML and the ESL technique especially at small wave numbers. The differences are attributed to spurious scattering in the EML. We have shown that this effect has only a minor influence on the analysis of the short-range order of the liquids. Nevertheless, the observed differences may be relevant when comparing the results with MD data. The development of the ESL furnace for neutron scattering results in a significant improvement of the quality of the measured structure factors at small momentum transfer.

ACKNOWLEDGMENTS

The authors thank M. Fiedler, F. Kargl, S. Klein, and I. Pommrich for support during preparation and performance of the experiments. We thank F. König for the design of the vacuum chamber and S. Schneider for the support in using the video analyzing software.

*Dirk.Holland-Moritz@dlr.de

[1] T. Voigtmann, A. Meyer, D. Holland-Moritz, S. Stüber, T. Hansen, and T. Unruh, Europhys. Lett. **82**, 66001 (2008).
[2] A. Meyer, Phys. Rev. B **81**, 012102 (2010).
[3] D. M. Herlach, R. F. Cochrane, I. Egry, H. J. Fecht, and A. L. Greer, Int. Mater. Rev. **38**, 273 (1993).
[4] D. L. Price, High-temperature Levitated Materials (Cambridge University Press, Cambridge, England, 2010).
[5] T. Schenk, D. Holland-Moritz, V. Simonet, R. Bellissent, and D. M. Herlach, Phys. Rev. Lett. **89**, 075507 (2002).
[6] D. Holland-Moritz, T. Schenk, P. Convert, T. Hansen, and D. M. Herlach, Meas. Sci. Technol. **16**, 372 (2005).
[7] C. Landron, L. Hennet, T. E. Jenkins, G. N. Greaves, J. P. Coutures, and A. K. Soper, Phys. Rev. Lett. **86**, 4839 (2001).
[8] L. Hennet *et al.*, Rev. Sci. Instrum. **77**, 053903 (2006).
[9] A. Meyer, S. Stüber, D. Holland-Moritz, O. Heinen, and T. Unruh, Phys. Rev. B **77**, 092201 (2008).
[10] S. Krishnan, L. Hennet, S. Jahn, T. A. Key, P. A. Madden, M. L. Saboungi, and D. L. Price, Chem. Mater. **17**, 2662 (2005).
[11] S. Ansell, S. Krishnan, J. K. Richard Weber, J. J. Felton, P. C. Nordine, M. A. Beno, D. L. Price, and M. L. Saboungi, Phys. Rev. Lett. **78**, 464 (1997).
[12] H. Kimura *et al.*, Appl. Phys. Lett. **78**, 604 (2001).
[13] C. Notthoff, B. Feuerbacher, H. Franz, D. M. Herlach, and D. Holland-Moritz, Phys. Rev. Lett. **86**, 1038 (2001).
[14] D. Holland-Moritz, T. Schenk, R. Bellisent, V. Simonet, K. Funakoshi, J. Merino, T. Buslaps, and S. Reutzel, J. Non-Cryst. Solids **312–314**, 47 (2002).
[15] G. Jacobs, I. Egry, K. Maier, D. Platzek, J. Reske, and R. Frahm, Rev. Sci. Instrum. **67**, 3683 (1996).
[16] G. Jacobs, I. Egry, D. Holland-Moritz, and D. Platzek, J. Non-Cryst. Solids **232–234**, 396 (1998).
[17] W. K. Rhim, S. K. Chung, D. Barber, K. F. Man, G. Gutt, A. Rulison, and R. E. Spjut, Rev. Sci. Instrum. **64**, 2961 (1993).
[18] S. Klein, D. Holland-Moritz, and D. M. Herlach, Phys. Rev. B **80**, 212202 (2009).
[19] K. F. Kelton, G. W. Lee, A. K. Gangopadhyay, R. W. Hyers, T. J. Rathz, J. R. Rogers, M. B. Robinson, and D. S. Robinson, Phys. Rev. Lett. **90**, 195504 (2003).
[20] G. W. Lee, A. K. Gangopadhyay, K. F. Kelton, R. W. Hyers, T. J. Rathz, J. R. Rogers, and D. S. Robinson, Phys. Rev. Lett. **93**, 037802 (2004).
[21] H. Aoki, P.-F. Paradis, T. Ishikawa, T. Aoyama, T. Masaki, S. Yoda, Y. Ishii, and T. Itami, Rev. Sci. Instrum. **74**, 1147 (2003).
[22] S. Earnshaw, Trans. Cambridge Philos. Soc. **7**, 97 (1842).
[23] T. Meister, H. Werner, G. Lohöfer, D. Herlach, and H. Unbehauen, Contr. Eng. Pract. **11**, 117 (2003).
[24] T. Unruh, J. Neuhaus, and W. Petry, Nucl. Instrum. Methods Phys. Res. A **580**, 1414 (2007).
[25] T. Unruh, A. Meyer, J. Neuhaus, and W. Petry, Neutron News **18**, 22 (2007).
[26] D. Holland-Moritz, S. Stüber, H. Hartmann, T. Unruh, T. Hansen, and A. Meyer, Phys. Rev. B **79**, 064204 (2009).
[27] A. Meyer, W. Petry, M. Koza, and M. P. Macht, Appl. Phys. Lett. **83**, 3894 (2003).
[28] A. Meyer, Phys. Rev. B **66**, 134205 (2002).
[29] J.-P. Hansen and I. McDonald, Theory of Simple Liquids (Academic, New York, 1976).
[30] J. Boon and S. Yip, Molecular Hydrodynamics (McGraw-Hill, New York, 1980).
[31] A. Meyer, J. Wuttke, W. Petry, O. G. Randl, and H. Schober, Phys. Rev. Lett. **80**, 4454 (1998).
[32] S. A. Chathoth, A. Meyer, M. M. Koza, and F. Juranyi, Appl. Phys. Lett. **85**, 4881 (2004).
[33] T. C. Hansen, P. F. Henry, H. E. Fischer, J. Torregrossa, and P. Convert, Meas. Sci. Technol. **19**, 034001 (2008).
[34] H. H. Paalman and C. J. Pings, J. Appl. Phys. **33**, 2635 (1962).
[35] G. Placzek, Phys. Rev. **86**, 377 (1952).
[36] T. Schenk, V. Simonet, D. Holland-Moritz, R. Bellisent, T. Hansen, P. Convert, and D. M. Herlach, Europhys. Lett. **65**, 34 (2004).
[37] S. Krishnan, J. J. Felton, J. E. Rix, J. K. R. Weber, P. C. Nordine, M. A. Beno, S. Ansell, and D. L. Price, Rev. Sci. Instrum. **68**, 3512 (1997).